PROCEEDINGS, 44th Workshop on Geothermal Reservoir Engineering
Stanford University, Stanford, California, February 11-13, 2019
SGP-TR-214

Umatilla Indian Reservation Geothermal Resources Assessment – Phase I

Geoffrey Garrison[1], Michael Swyer[2], Trenton Cladouhos[2], Brent Ritzinger[3], Jared Peacock[3], Carl Palmer[4], Jonathan Glen[3], Richard Blakely[3], Patrick Mills[5]

[1]Hot Rock Energy Research Organization (HERO), 4010 Stone Way North, Suite 400, Seattle, WA 98103

[2]formerly at AltaRock Energy, now at Cyrq Energy Inc., 4010 Stone Way North, Suite 400, Seattle, WA 98103

[3]US Geological Survey, 345 Middlefield Rd., Menlo Park, CA 94025

[4]560 NW Silverado Dr., Beaverton, OR 97006

[5]CTUIR-DNR Energy & Environmental Sciences Program, 46411 Timine Way, Pendleton, Oregon 97801

ggarrison@hotrockenergy.org

Keywords: geothermal resource assessment, geophysical data integration, multicomponent geothermometry, geothermal resource favorability, resource potential, thermal gradient borehole targeting, play fairway analysis, analytical hierarchy process

ABSTRACT

This report concludes the work accomplished during the first phase of evaluating the geothermal resource potential of the Umatilla Indian Reservation (UIR). The project was a coordinated effort between the Confederated Tribes of the UIR (CTUIR), HotRock Energy Research Organization, AltaRock Energy, and the USGS. Reconnaissance and data collection activities included geologic field visits; paleomagnetic and rock property sampling; gravity, magnetic, and magnetotelluric geophysical surveys; and groundwater geochemical analysis. Data was refined and modeled using state of the art methodology and software. This included using the chemical properties of water samples as inputs to multicomponent geothermometry so that temperatures at depth could be estimated. Resource favorability maps were rendered based on integrated data, and they will guide subsequent phases of geothermal exploration. The ultimate goal of this work is to develop resources for direct-use (heating) and/or power production for the benefit of the Cayuse, Umatilla and Walla Walla Tribes.

Located in northeastern Oregon on the northwest flank of the Blue Mountains, the UIR is situated near the intersection of the two major regional fault systems: 1) the Klamath-Blue Mountains Lineament (KBL) which extends southwest across the Klamath Mountains in southwestern Oregon, and 2) the Olympic-Wallowa Lineament (OWL) which extends west-northwest to the Puget Lowland in northwestern Washington. Located in the UIR, the Thorn Hollow, Hite, and Wilahatya faults are major linkages between the KBL and the OWL and are considered important structures for controlling fluid flow. Geophysical surveys identified the location and structure of these and numerous smaller-scale structures which may influence fluid flow and geothermal favorability.

The geophysical, geologic, and geochemical data were integrated into a geothermal resource potential model using the methodology of the 2017 Washington State Play Fairway Analysis (PFA). Data were grouped into three categories of geothermal resource indicators: 1) heat, 2) permeability, and 3) presence of fluids or a cap. Data were normalized and weighted based on geothermal favorability using an expert-opinion, team-based Analytical Hierarchy Process (AHP) and then loaded into a GIS mapping platform to determine the relative position of resource indicators across the UIR. Overall geothermal favorability was mapped across the UIR based on combined AHP weighted data, and eight locations were identified as the most favorable for further resource investigation.

A speculative model of the hydrothermal system below the UIR is presented and serves as a hypothesis to evaluate future new field data (e.g., thermal gradient boreholes). The model begins with meteoric water infiltration in the highlands of the Blue Mountains. As that water descends, primarily through deep-seated crustal faults and major fault intersections, the water heats up, becomes buoyant, and migrates northwest away from the mountains into the central area of the UIR – the region identified as having higher geothermal favorability. Zones along the Wilahatya fault system may tap deep thermal reservoir fluids at fault intersections and provide potential access to those fluids at relatively shallow depths. It is those zones that have been identified as the most favorable locations for further exploration. Findings indicate a potentially viable geothermal resource for which further investigation is necessary to confirm. As such, proceeding with additional Geothermal Resources Assessment work is strongly recommended, particularly drilling exploratory temperature gradient holes to depths of 1.5 to 2.5 km.

1. INTRODUCTION

The Umatilla Indian Reservation Geothermal Resources Assessment project was initiated by the Confederated Tribes of the Umatilla Indian Reservation (CTUIR) with the objective of completing the first technical evaluation of the subterranean thermal resource potential of the Umatilla Indian Reservation (UIR). This report presents the results, findings, and conclusions of the first

phase of the project, referred to as to as UIR Geothermal - Phase 1, to characterize geothermal resource favorability and guide subsequent phases of exploration with the ultimate goal of developing identified resources for direct-use (heating) and/or power producing applications. Additional exploration would include further geophysical data collection, and/or thermal gradient holes to confirm the presence of an economically viable geothermal resource and would provide the information necessary for designing a system to harness that resource for the benefit of the CTUIR.

This work focused on terrestrial and aerial geophysical surveys in addition to geochemical analysis of groundwater sources of interest so that future costs and risk could be minimized. Specific tasks completed during the 15-month (2017-18) project included:

- Compiling and refining existing data relevant to the project;
- Gravity survey with data collected at 1,384 new stations;
- Magnetic surveys covering an area of 12,524 km2 (34,524 line-km);
- Magnetotelluric survey with data collected at 36 new stations;
- Paleomagnetic and rock property sampling;
- Geochemical analysis of 60 analytes and parameters in 24 unique springs and wells;
- Multi-component geothermometry using the geochemical data set; and
- 2-Dimensional and 3-Dimensional potential field modeling.

To complete a project of such broad technical scope, the expertise of a diverse team was assembled consisting of CTUIR scientists and engineers, United States Geological Survey (USGS) researchers, and geochemists and geothermal industry developers from Hotrock Energy Research Organization (HERO) and AltaRock Energy, Inc. (ARE). USGS geophysicists led data collection efforts and assisted with modeling and interpretation of the results. ARE was contracted by HERO to serve as a geothermal consultant and was responsible for assisting with field work and integrating the USGS geophysical survey results into a conceptual model with which the geothermal resource favorability within the UIR could be quantified.

2. BACKGROUND

The CTUIR has actively pursued development of renewable energy projects for many years including previous wind and solar projects. The CTUIR now seeks to develop potential geothermal resources particularly because such projects have minimal impacts to wildlife migration, cultural resources, and viewshed.

2.1 Geology and Tectonics of the Blue Mountains

The Blue Mountains cover ca 10,500 km^2 in northwest Oregon with elevations in places exceeding 2,000 m. They are thought to be underlain primarily by the Wallowa volcanic arc terrane, a composite block consisting of a Permian island-arc sequence overlain by extensive Triassic volcanic and volcaniclastic rocks (Schwartz, J. et al. 2009). Most of the Blue Mountains are composed of surficial lava flows and dikes of the Columbia River Basalt Group (CRBG), particularly the Grande Ronde Basalt which erupted ca 16.5 million years ago (Mya) (Barry et al. 2013). Sedimentary interbeds lie between basalt flows in some of the low-lying basins. Uplift of the Blue Mountains orogeny is attributed to north-south horizontal tectonic stresses. Due to uplift, late-stage CRBG flows did not cover the emerging Blue Mountains but rather onlap the margins of the range. Folding and faulting ca 12 to 10 Mya is associated with horizontal north-south compression accompanying the uplift. Uplift of the Blue Mountains has subsequently caused the surrounding rivers (i.e., Grande Ronde, Tucannon, John Day, Umatilla, and Walla Walla) to carve deep canyons through CRBG units and into the underlying geology.

The Hite fault system lies near the intersection of two regional-scale, structural lineaments: the northeastern end of the Klamath-Blue Mountains Lineament, which extends southwestward to southwestern Oregon, and the Wallula fault, the southeastern end of the west-northwest trending Olympic-Wallowa Lineament that extends to the Olympic Peninsula (Figure 1). Quaternary faults in and near the UIR are part of the Hite fault system and exhibit left-lateral strike-slip displacement (U.S. Geological Survey Quaternary Fold and Fault Database—QFFDB). The UIR location at the intersection of two regional fault systems indicate promising geothermal potential for the area. The Grande Ronde Valley fault system southeast of the UIR is surrounded by north-northwest trending normal faults that form an extensional graben that contains the Hot Lake Springs (average temperature of 93° C). Tectonic stresses are relatively low within the UIR compared to the western United States.

3. GEOTHERMAL RESOURCE DATA

A geothermal reservoir requires that heat, saturated porosity, permeability, and an impermeable cap be collocated at drilling-accessible depths and are sufficient enough to supply adequate heat to the surface. The volume of permeability and the intensity of fracturing in combination with the temperature at depth determine the commerciality of the resource by defining the volumetric heat, in-place heat, and the recovery factor. This project generated maps indicating the relatively most favorable areas where heat, structural permeability and overlying reservoir cap and/or fluids are collocated in the UIR.

Data collection and assessment was a coordinated effort between HERO, ARE, the CTUIR, and the USGS. The USGS completed magnetotelluric (MT), high-resolution aeromagnetic, and gravity geophysical surveys. CTUIR managed the project and was responsible for groundwater sampling. Samples were split and preserved according to target analyte/method and distributed to

participating laboratories including the ORELAP accredited CTUIR Field Station. ARE and HERO were responsible for reviewing and assessing the data collected by the USGS and CTUIR with respect to geothermal resource potential, and was responsible for integrating geologic, geochemical and geophysical data into a model of geothermal favorability to locate accessible geothermal resources within the bounds of the UIR. Heat potential maps were generated by compiling data on hot springs, geothermometry from groundwater chemistry, and wells with measured heat flow. Permeability potential maps were generated by compiling data on faults, crustal movements from geodetic strain rates, and far-field stress indicators to determine fault density and fault slip/dilation tendency. High electrical conductivity, revealed by MT data, can indicate clay alteration and potentially a geothermal reservoir cap at shallow depths and potentially saline geothermal brines at depth. The mapped results of heat, permeability, cap, and fluid potential are combined into geothermal favorability maps by weighting them in a quantitative expert opinion approach.

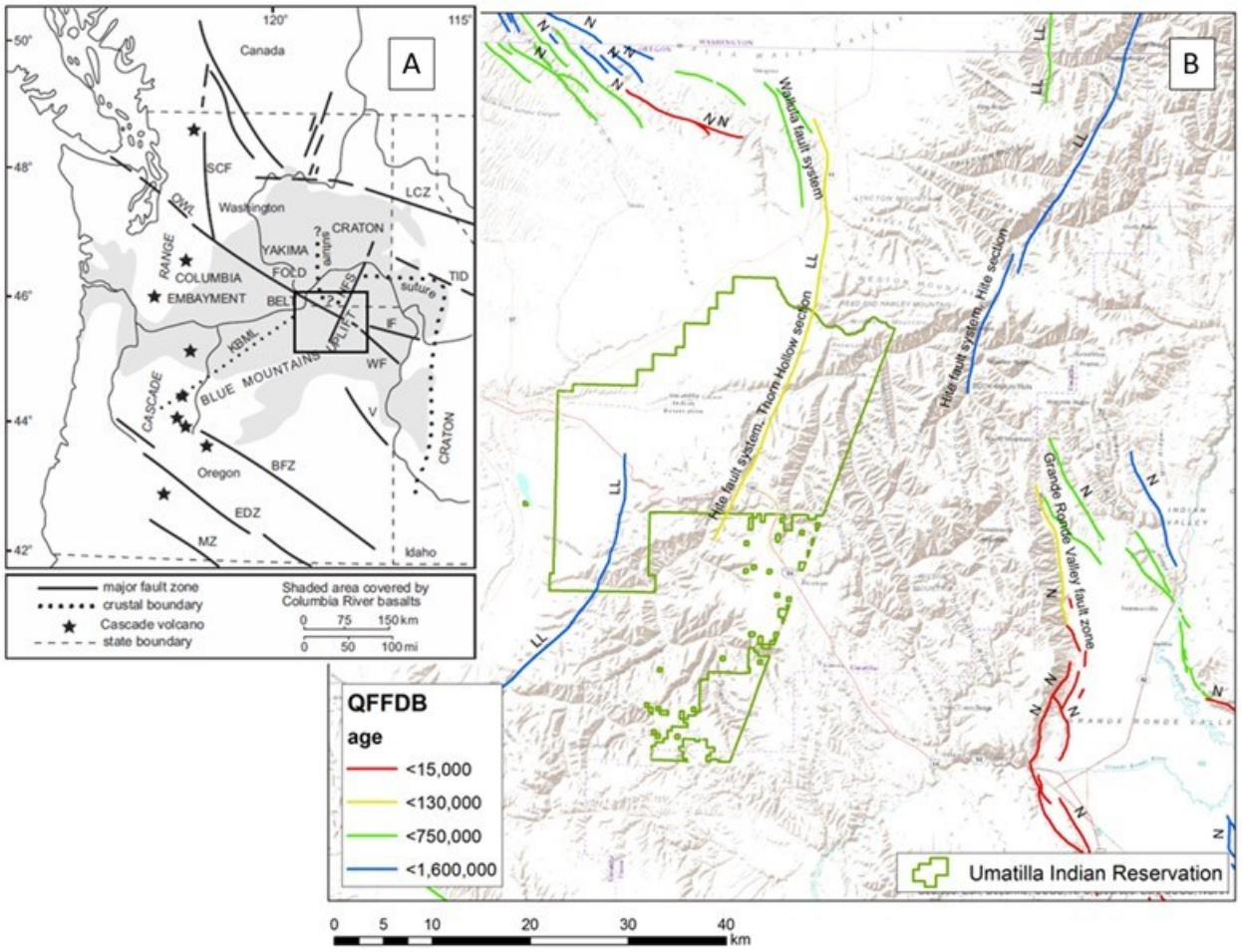

Figure 1: (A) General location map of the study area (Modified from Kuehn, 1995). (B) Quaternary faults around the UIR colored by age and labeled by sense of slip: N = normal faulting and LL = left-lateral strike-slip. Source: USGS Quaternary fault and fold database. The green polygons define the borders of the UIR.

3.2 Tectonics

3.2.1 Stress/Strain regime

Crustal motion across the Pacific Northwest region has been measured by Global Positioning System (GPS) measurements relative to benchmarks in the stable North American craton (McCaffrey et al., 2007). The Cascadia Subduction Zone creates a unique tectonic stress regime that developed clockwise rotation on shallow crustal blocks across the Pacific Northwest. The UIR is located near the central axis of the regional rotating blocks and has some of the lowest velocities in the Pacific Northwest relative to the stable North America reference frame, but there is some tectonic motion that can maintain fault permeability. Figure 2 shows the location of strain-rate tensors which constrain the stress regime for the UIR derived from GPS benchmarks from the Pacific Northwest Geodetic Array (PANGA) for every 0.04° longitude and 0.10° latitude (McCaffrey et al., 2007). Also shown are recently active faults identified in the QFFDB.

Both principal strain-rates (ε_H and ε_h) are low in magnitude and compressive; the rate across the UIR is less than 0.5% of the maximum regional compression. The average compressive strain-rate is oriented 43° East of North and is perpendicular to the crustal block boundary defined by McCaffrey et al. (2007) that runs through the UIR, presumably activated by episodic release of stress along a deep-seated plane of weakness in the continental crust. Strain is a measure of local crustal deformation and may not be an accurate indicator of regional north-south compression, but it is useful for constraining relative stress magnitudes to determine the stress regime for the UIR, which is thrust faulting transitional to strike-slip faulting. To constrain the remote stress direction, the average strain-rate tensor was transformed to an average orientation for geomechanical analysis of faulting in the UIR using the World Stress Map database (Heidbach et al., 2016).

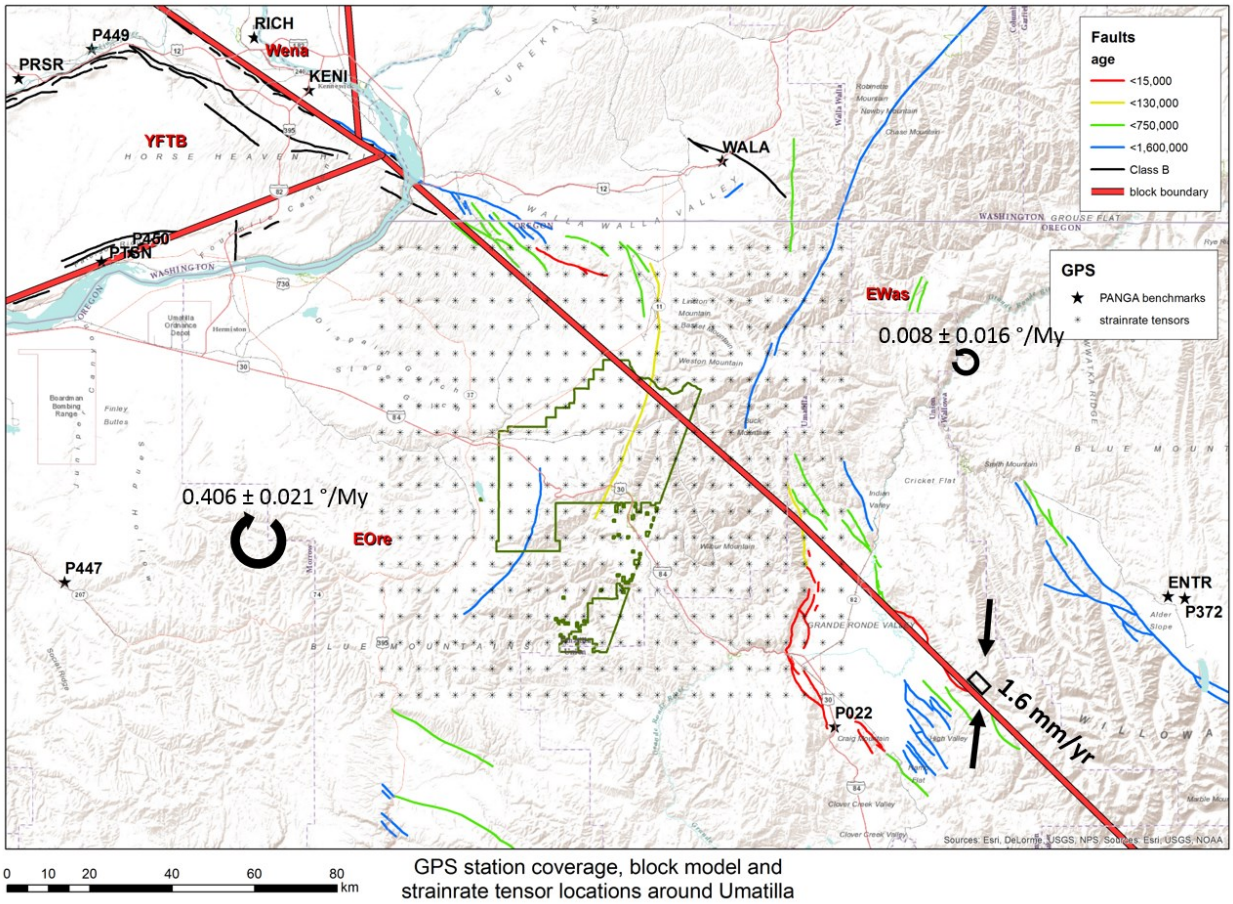

Figure 2: Strain-rate tensor solutions to assess stress regime. Also shown: GPS benchmark locations (stars), block boundary with displacement rate and vector (based on McCaffrey et al., 2007), rotation rates for the two blocks surrounding the UIR, and faults and fold axes from the QFFDB by age.

3.2.3 Active Faults and Seismotectonics

Most of the stress indicators in the World Stress Map database near the UIR are earthquake focal mechanisms to the northwest that indicate strike-slip and thrust faulting stress, with some indicators of normal faulting further away to the southeast (Figure 3a). The stress data were queried within a radius of 350 km to obtain a robust constraint on the stress orientation using the MATLAB script Stress2Grid.m, which creates a smoothed grid of stress orientations. It was used to solve for stress at the same location as the strain-rate tensors shown in Figure 2. The mean stress orientation for the UIR is 6.5° east of north (Figure 3b), which agrees with the direction of motion on the crustal block boundary that runs through the UIR in McCaffrey's model (Figure 2). Variable stress indicators for the area surrounding the UIR can be attributed to the fact that tectonic stress magnitudes in this area are relatively low for the western United States. As described below, the low tectonic stress magnitudes led the team to give stress parameters relatively low weights in overall geothermal favorability compared to other geothermal assessments.

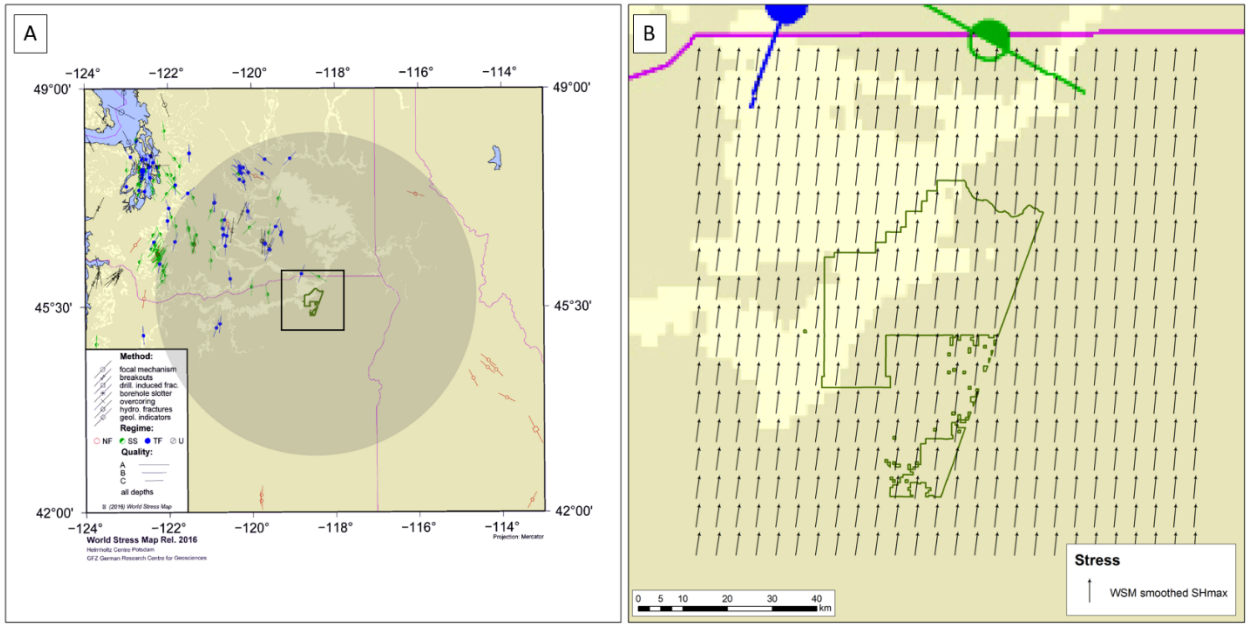

Figure 3. World Stress Map data around the UIR. (A) larger map with darker circle representing where the database was queried to create smoothed stress orientations shown in (B).

3.2.4 Stress on Faults

After the 2D strain-rate tensor was transformed to the stress orientation from the World Stress Map, the vertical component was calculated using Hooke's Law with a Poisson ratio (ν) of 0.25:

$$\varepsilon_V = -\nu\left(\varepsilon_H + \varepsilon_h\right) \qquad \text{eq. 1}$$

The strain rate magnitudes in units of micro-strain per year (μ-strain/yr) were multiplied by a Young's modulus of 30 Gigapascal (GPa) to get stress magnitudes, which were normalized for a vertical stress equivalent to the weight of overlying rock at depth using a rock density of 2.0 g/cm^3 for the initial 200 m below the surface representing unconsolidated rock and soil, and 2.8 g/cm^3 typical for basalt. The rock parameters used to get stress magnitudes from geodetic strain-rates are assumed as typical values for rocks and are not specific to the rock types for the area. The relevant attributes of the stress for slip and dilation tendency analysis on faults is the orientation which is well constrained by the World Stress map data, and the relative magnitudes of the principal horizontal stresses which are well constrained by the geodetic strain-rate data.

3.3 Geophysical Surveys

Potential-field (gravity and magnetic) measurements and magnetotelluric data are ideally suited for imaging geologic units and structures reflecting lateral variations in rock density, magnetic properties (magnetic susceptibility and remanent magnetization), and electrical resistivity. Such contrasts may derive from a variety of causes, such as facies changes within a single rock unit, changes across geologic structures such as faults and folds, or at contacts between distinct rock units. These lateral geologic discontinuities result in potential-field variations, or anomalies, that relate to the shape, depth, and rock-properties of the source rocks. Potential-field methods, therefore, are very effective in resolving subsurface lithology and structure, particularly when combined with other geologic and geophysical data.

Potential-field methods are useful in geothermal settings, as they can resolve structural features, such as contacts, faults and fracture zones that may play a significant role in transmitting geothermal fluids, or that may be activated during stimulation of a geothermal field. A potential field approach is particularly useful in the inland Pacific Northwest where flows of the Columbia River Basalts Group (CRBG) lava flows obscure much of the pre-Miocene geology and tectonism. The strong magnetic signature of CRBG flows make shallow structures especially easy to identify, while gravity measurements help further facilitate the modeling of deeper structures and contacts.

The USGS acquired and analyzed gravity, aeromagnetic, and magnetotelluric data to construct detailed 2-D profile models to assess potential geothermal fluid reservoirs and resolve structures that may be responsible for migration of geothermal fluids beneath the UIR (Peacock et al., 2018; Ritzinger et al., 2018). An overview and key findings of these surveys are summarized in this report. Data sources employed in this study include:

- approximately 350 existing gravity stations;
- 1,384 new gravity measurements;
- 54 hand samples measured for density and magnetic susceptibility;
- 647 outcrop samples measured for magnetic susceptibility;
- 56 paleomagnetic core samples from 17 CRBG flows measured for remanent magnetization;
- 34,524 line-kilometers of new aeromagnetic data; and
- MT data collected at 36 stations.

3.3.1 Gravity Survey

The gravitational attraction of the earth depends in part of the density of upper-crustal rocks. Thus, lateral variations in gravity are directly related to geologic structure. Gravity data for this study were acquired by the USGS between May and June 2017 using a Scintrex CG5 Gravity Meter. A database of approximately 350 gravity stations spanning an area of ca 110x110 km, which included the entire UIR area, was extracted from a public domain dataset, reprocessed, and combined with newly acquired gravity stations. The USGS acquired 1,380 new gravity stations in the study area, sampled in a grid pattern, at 1600 m intervals when possible, and along detailed (400- to 200-m spacing) profiles crossing major structures. The gravity measurement distribution for this survey was designed to fill regional gravity coverage while collecting detailed transects across known, through-going faults within the study region. All gravity data were tied daily to primary base stations in Pendleton, OR, or Walla Walla, WA, and both base stations were tied to the absolute gravity base station *Pendleton CA* (observed gravity of 980,331.704 ± 0.003 mGal). The gravity compilation provides exceptional regional coverage of the UIR Geothermal study area. It also provides detailed control on the location of major faults, constrains the thickness of underlying sediments of the Clarno formation and helps identify variations in crustal composition (Ritzinger et al., 2018).

3.3.2 Aeromagnetic Survey

Rocks possess two types of magnetization. Induced magnetization is induced by the earth's magnetic field in the direction of and proportional to the intensity of the external field. Remanent magnetization, on the other hand, is a long-term, in situ property of the rock, often related to the rock's thermal history and polarity of the magnetic field when the rock was formed. In unmetamorphosed volcanic rocks, such as most of the CRBG basalts, remanent magnetization is many times stronger than induced magnetization.

Like gravity, lateral variations in magnetic properties produce anomalies in the magnetic field that can be interpreted with respect to geologic structure. 34,524-line kilometers of magnetic data were acquired via Cessna 180 aircraft (i.e., "aeromagnetics") by EDCON-PRJ, Inc., from June to August 2017. The survey covered 12,524 km^2 encompassing the entire UIR study area. The survey was flown on a surface nominally draped 200 m above terrain, except in areas of rugged terrain. Primary survey lines were directed ca E-W and spaced 400 m apart; ca N-S tie-line were spaced 4,000 m apart. New survey data were merged with existing high-resolution aeromagnetic data previously collected to the north of the UIR. A base station magnetometer was set up just west of the Pendleton Airport to record temporal changes in the ambient magnetic field. Base station data were used to make diurnal corrections to the observed aeromagnetic data (Ritzinger et al., 2018).

3.3.3 Magnetotelluric Survey

Magnetotellurics (MT) is a passive electromagnetic geophysical method that measures the Earth's electrical response to naturally varying magnetic fields. Electrical currents are induced as these magnetic field variances diffuse into the subsurface. Depth of penetration of the diffusing magnetic field depends on subsurface electrical resistivity and the frequency of the inducing magnetic field. Thus, the Earth's electrical response contains information about subsurface features with differing resistivity such as sediments, clays, rocks, fractures, and fresh or saline fluids. MT was measured in the field by using induction coils to measure the time-varying magnetic source for frequencies between 1,000–0.001 Hz, and electric dipoles to measure the Earth's electrical response. MT data was collected at 36 stations with a ZEN 32-bit data logger developed by Zonge International. The data was collected on a repeating schedule of 5 min at 4096 samples/s and 7 hours and 55 minutes at 256 samples/s over a 20 to 24-hour period (Peacock et al., 2018).

3.3.4 Summary of Faulting Interpretation Based on Geophysics

Gravity and aeromagnetic data were processed and filtered using standard routines available in Oasis Montaj® software, and new data were merged with existing datasets (Ritzinger et al., 2018). MT response functions were modeled in three-dimensions (3-D) using the code ModEM. Multiple conductive and resistive anomalies are present in the preferred 3D electrical resistivity model (Peacock et al., 2018).

The study area encompasses a region where two major crustal-scale lineaments interact: the NE-trending Klamath-Blue Mountain lineament (KBL) and the SE-trending Olympic-Wallowa lineament (OWL). The geologic cross-section analyses across the study area presented in Ritzinger et al., 2018, includes the modeling of three primary lithologic groups: CRBG, the underlying generalized sedimentary unit representing the Clarno Formation, and the basement. The KBL and OWL manifest locally as numerous sub-parallel structures. The NE to NNE-trending Hawtmi fault at the eastern margin of the Pendleton basin and western edge of the Blue Mountains is the local expression of the KBL. The NE-trending Thorn Hollow and Hite faults and the ENE-trending Wilahatya

fault zone – major linkages between the KBL and the OWL – run through the UIR and are considered important structures controlling geothermal fluid flow. The geophysical data reflect the location and structure of these faults and reveal numerous smaller-scale structures which can influence subsurface fluid migration and impact geothermal favorability.

A general trend was described from the MT data in Peacock et al., 2018: a more resistive cover less than 1,500 m thick—interpreted as a combination of alluvium sediment cover and Miocene Columbia River basalts—overlays a more conductive 1–4 km thick layer that plunges to the southwest. The Peacock resistivity model shows conductive zones along the Wilahatya fault near the intersection margins with the Thorn Hollow fault, Hawtmi fault, and an unnamed "Fault A". Such fault interactions commonly reflect zones of enhanced permeability that promote fluid flow. The intersection of the Thorn Hollow and Wilahatya faults appears structurally complex with enhanced conductivity 400-2,000 m below mean sea level (BMSL). The Thorn Hollow fault is observed to have left oblique motion possibly down dropped to the west, and the Wilahatya has normal motion. The intersection of Fault A and the Wilahatya fault has a zone of enhanced conductivity 1,000-3,000 m BMSL, which is slightly deeper than that associated with the Thorn Hollow intersection. Similarly, there is a conductive zone near the intersection of the Wilahatya and the Hawtmi faults 2,000-5,000m BMSL, which is even deeper still than conductive zones associated with fault intersections to the east (Peacock et al., 2018).

3.4 Aquatic Geochemistry and Geothermometry

Samples of groundwater were collected across the UIR from both surface springs and wells. Inorganic groundwater chemistry was analyzed to predict subsurface temperatures, to understand the pattern of circulation for geothermal fluids, and provide information on their origin (Palmer, 2018). The analysis process assumes the waters were once in chemical equilibrium with surrounding rocks and minerals promoted by heat within the reservoir. Traditional geothermometers are mineral-specific and only compare a subset of dissolved chemical constituents with respect to a few potential minerals. However, while thermal fluid chemistry is largely controlled by reservoir temperature and mineral assemblage, processes such as cooling, mixing, or degassing can also impact chemical composition. Thus, geothermometer interpretation is a complex problem often providing non-unique results. However, this study estimated temperatures at depth using more recent multicomponent chemical geothermometry methods. This technique uses the full suite of chemical analyses for each sample and calculates reservoir temperature based on the saturation indices for a group of potential reservoir minerals (Palmer, 2018).

Groundwater sources were sampled across the project area under guidance of the CTUIR's Sampling and Analysis Plan (CTUIR, 2017) in accordance with ASTM Standard D4448. A total of 26 parent samples (not including quality control samples) were collected from 18 groundwater wells and six surface springs shown on Figure 8. Samples were distributed to three analytical laboratories; the CTUIR Field Station, USGS Menlo Park Science Center, and USGS Reston Stable Isotope Laboratory (RSIL). Geothermometries were interpreted using the Reservoir Temperature Estimator (RTEst) software package. RTEst minimizes the weighted sum of squares of the saturation indices of selected minerals believed to be in equilibrium with the waters tested by adjusting the temperature, carbon dioxide fugacity (fCO_2), water mass, or mixing with meteoric water that hasn't been geothermally affected. RTEst uses the React module in The Geochemist's Workbench (GWB) to do the geochemical calculations while model parameters were optimized using the PEST commercial software package for parameter estimation and uncertainty analysis. A modified version of the GWB thermo.tdat database was used for thermodynamic equilibria. The mineral assemblages considered were based on studies of geologic formations located in the Columbia Plateau of western Washington. Although mineralogical studies specific to the study area have not been conducted, several studies of the basalts of the Columbia River plateau were used for guidance during mineral suite selection.

3.4.1 Cluster Analysis

Before the aquatic chemistry data were scrutinized, it was determined whether there are chemically similar subgroups of samples within the whole collection using a hierarchical cluster analysis process (Palmer, 2018). Grouping the samples helps to both select appropriate mineral assemblage for the geothermometry analysis and provide insight into fluid origins and circulation. The analytes used for the cluster analysis included Cl, F, Br, SO_4, Al, B, Ba, Ca, Fe, Ge, K, Li, Mg, Mn, Mo, Na, V, Zn, and alkalinity. Analytes that were below the reporting limit were assigned a value equal to half of reporting limit; assigning one half the reporting limit value does not significantly impact the cluster analysis results but does prevent zero-value errors in processing. The hierarchical cluster analysis was performed on normalized data with Statistica™ (version 13.0) software package.

Four Groups among the sample were identified using Ward's method (Figure 8). The criterion used to define the Groups is a minimum distance value between clusters. A criterion value of 58.27 was used here which is the mean cluster distance value plus a constant *k* times the standard deviation of the population; a *k* of 1.25 was used in this study (Palmer, 2018). The four Groups are shown in Figure 8 and dicussed in the following sections of this report. Group 1 consists of one sample, Geo.S2-XXX-170928, which was collected from Bingham Springs and is located just east of the UIR along the Umatilla River valley. Group 3 locations (7) are the most elevated sites and are found in the west and southwest of the study area. Group 2 locations (5) are farthest away from the Blue Mountains and located out on the farmlands in the northwest of the UIR. Group 4 locations (12) are found primarily along the base of the Blue Mountains on a northeast-southwest trend between the locations of Group 3 and Group 2.

3.4.2 Groundwater Chemistry

Figure 5 illustrates box-and-whisker plots of dissolved chemistry sorted by Group. Groups 2, 3, and 4 span the same relative composition of major cations, have total dissolved solids (TDS) between 130 and 580 mg/L, and are characterized as being Ca-Mg-Na-HCO_3 to Na-HCO_3 waters, while Bingham Springs is a Na-Cl water (Figure 6). In addition to dissolved Na^+, Ca^{2+}, and Mg^{2+}, silica ($SiO_{2(aq)}$) is also a significant dissolved constituent as illustrated in a Na-$SiO_{2(aq)}$-Ca ternary diagram (Figure 6).

Groundwater beneath the UIR appears to evolve in a fashion similar to that seen elsewhere in the Columbia Plateau. Group 3 waters appear to represent meteoric water infiltrating the subsurface in the higher elevations of the Blue Mountains. As this water descends, it acquires CO_2 which reacts with the basalt dissolving volcanic matrix, pyroxenes, and possibly olivine, which releases cations and $SiO_{2(aq)}$. Eventually amorphous forms of Al, Mg, SiO_2, and smectite clays (primarily as nontronite) precipitate as ion concentrations continue to rise. Increasing pH and concentrations of Ca^{2+} due to the silicate mineral hydrolysis results in calcite precipitation. Eventually, clinoptilolite and mordenite precipitate as concentrations of Na^+, K^+, and $SiO_{2(aq)}$ continue to rise. It is speculated that as waters descend into the deep aquifers, becoming warmer due to heat flow from deeper in the Earth, then rise due to decreased density, and amorphous silica forms as ascending waters cool. This model is consistent with groundwaters beneath the UIR being in equilibrium with calcite, amorphous ferric oxides, allophane, and amorphous SiO_2 which is supported by the geothermometry analyses described below.

Based on this model, the Groups appear to represent different stages within the flow path of groundwater beneath the UIR. Looking at TDS and geothermal indicator species Cl and Li, Group 3 are the most chemically immature waters (Figure 5) and show no significant evidence of geothermal influence. Group 3 samples are located at higher elevations than the other samples (Figure 8), and thus appear to represent early meteoric water infiltrating the subsurface. Group 4 samples are located more within the farmlands along the edge of the Blue Mountains, have a higher temperatures, Cl and Li and K concentrations, and thus appear to represent older waters moving through the aquifer system. Group 2 samples are located even farther from the Blue Mountains in wheat fields of the UIR. The reduced silica concentrations in these samples may indicate silica precipitation after this water has ascended and cooled following contact with hotter parts of the subsurface, thus retaining higher concentrations of conservative geothermal elements Cl^- and Li^+. Finally, Group 1, which is water from the nearest accessible hot spring to the UIR, Bingham Springs, is geothermally most mature. It's high concentrations of Li, Cl, P, Si, and especially B indicate that it has not mixed or cooled as much as waters samples in the other Groups. The chemistry of Bingham Springs water is closest to what could be expected to be produced from a geothermal reservoir in the subsurface beneath the UIR. Furthermore, the geothermometry analyses will demonstrate that the water coming from Bingham Springs is most closely related to the water samples in Group 2.

3.4.3 Modeled Reservoir Mineralogy

Selecting which minerals that should represent the heat reservoir is a key challenge to multicomponent equilibrium geothermometry. Although mineralogical studies specific to the study area have not been conducted, there are several studies of the basalts in the Columbia River plateau that provided guidance in selecting a mineral suite for the UIR study. The Columbia River Basalt Group lavas are tholeiitic and contain plagioclase, pyroxene, and metal oxides. Plagioclases vary from labradorite (30-50% albite) to andesine (50-70% albite), pyroxenes vary from augite to subcalcic augite, and secondary minerals are primarily clays, zeolites, and silica. Less abundant minerals include calcite, pyrite, gypsum, apatite and a variety of zeolites. Clays are iron-rich smectites and may include nontronite. Smectite is ubiquitous in vertical profiles on the Columbia Plateau, though usually less common at depths >600 m. Predominant zeolites include clinoptilolite and mordenite, and clinoptilolite is found at depths greater than 350 m. At depths >900 m some solution etching of clinoptilolites has been observed and mordenite appears less abundantly. Clinoptilolite taken from shallower depths has K and to a lesser extent Ca as the exchangeable cation while deeper samples are dominated by Na in the clay mineral exchange sites. Silica is present in the chalcedony, cristobalite, and opal, with chalcedony ubiquitous within all units and opal and cristobalite abundant at depths >600 m. Secondary minerals found in fractures are mostly clay, clinoptilolite, silica, and pyrite. Apatite, mordenite, chabazite, and erionite are generally only observed in vesicles. Celadonite has also been identified as a common alteration product in these basalts.

3.4.4 Geothermometry Results

Figure 7 is an example of how mineral saturation indices plotted against temperature for the reservoir mineral suite selected were used to calculate equilibrium temperature for water from Bingham Springs (Group 1). Figure 8 illustrates the temperature calculated (° C) at which the water in each sample equilibrated with the mineral suite selected for that sample in the optimization process.

Group 1. Bingham Springs (Group 1) data was optimized for temperature and CO_2 activity (i.e., CO_2 fugacity, or log[fCO_2]) using a mineral assemblage of cristobalite and clinoptilolite yielded a temperature of 111.4 ±0.2° C. This water is in equilibrium with several minerals that have either been specifically identified in these rocks or are reasonably expected in basalts.

Group 2. These waters are supersaturated with respect to amorphous silica when compared to the silica concentrations of the host basaltic rock. The calculated geothermometries of 24.5 to 33.9° C in most of these samples is 10 to 20° C warmer than their current state. Thus, it appears that these waters previously equilibrated at higher temperatures, where the solubility of SiO_2 is greater, and then cooled while kinetically maintaining their silica content. Other minerals near saturation include aragonite/calcite, analcime, high albite, celadonite, gibbsite, lawsonite, and gibbsite—minerals which either have been identified specifically in the basalts of

the region or their occurrence is probable for these rock types. Sample 1004-XXX-170926 gave ambiguous results and it was not included in calculating geothermal favorability. Group 2 waters may be impacted by irrigation water as indicated by higher levels of nitrate, sulfate, and total dissolved solids (Figure 5), especially since there are suggestions in graphs of mineral saturation versus temperature that these waters have been mixed. An exception in this group is the sample from Minthorn Springs; with a geothermometer of 94.2° C, this sample may be more related to waters at the Group 4 locations.

Group 3. Only two of the seven samples had reportable Al, and the other Al concentrations were computed by assuming equilibrium with high albite (i.e., analbite). Geothermometric calculations on Group 3 optimized for temperature for the minerals amorphous silica and high albite (using samples with Al greater than the reporting limit), or for amorphous silica and analcime (samples with Al less than the reporting limit), found equilibrium temperatures ranged from 18.3 to 32.2° C. These values may represent slight heating of groundwater, but it is not beyond what would be expected from the typical geothermal gradient found within the upper 5 kilometers of normal continental crust. These locations appear to be where rainfall and surface water is infiltrating into the subsurface.

Group 4. These samples yielded three general ranges of temperatures that loosely depend on the fraction of Na^+ in the water. Eight of the samples have Al concentrations greater than the reporting limit. Four of these samples appear to have geothermometric temperatures in the range of 37.4 to 47.9° C for a mineral suite that includes amorphous silica and either high albite or lawsonite. Two samples suggest equilibration with cristobalite and clinoptilolite-K with temperatures of 105.5 and 111.3° C. For the six samples with Al less than the reporting limit, the geothermometric temperatures ranged from 93.6 to 118.6° C. Many of the Group 4 locations align along the Wilahatya fault, which trends east-north-east along the Umatilla River valley and intersects Bingham Springs. The fault may relate all these waters since Group 4 and Bingham Springs both appear to equilibrate with the same mineral types and rock temperatures. However, the bulk compositions of these fluids are dissimilar, which could indicate that while the fault controls fluid flow from depth, the later flow paths and residence times of Group 4 and Bingham Springs are different. That is not surprising considering that the waters at Bingham Springs emanate directly from fractures in the bedrock exposed at the ground surface in the Umatilla River valley.

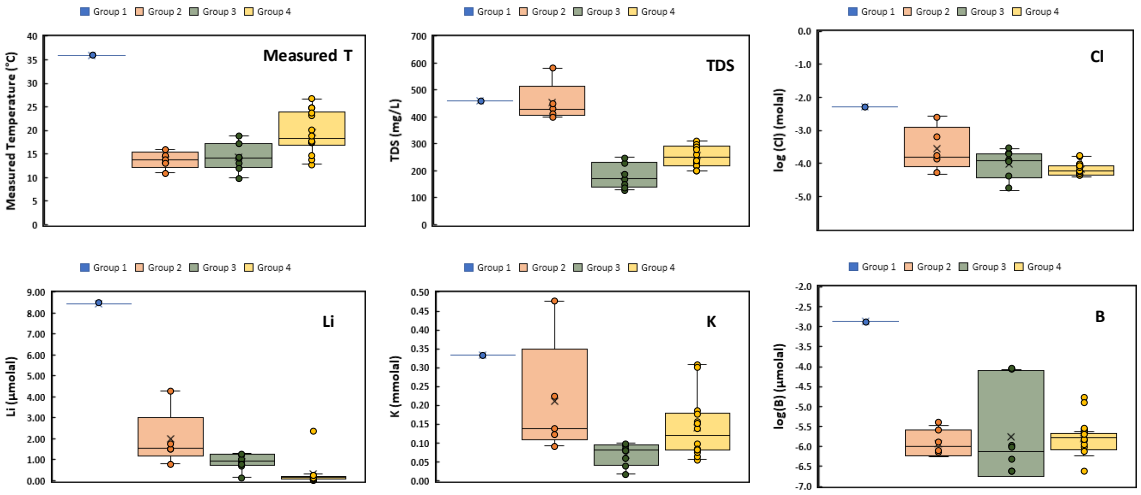

Figure 4. Box-and-whisker plot of groundwater chemistry in samples from Groups 1, 2, 3, and 4. Individual samples are represented by circles; boxes represent second quartile of each Group data with the median plotted as the horizontal line within each box; whiskers above and below each box represent 1st and 3rd quartiles of each Group data.

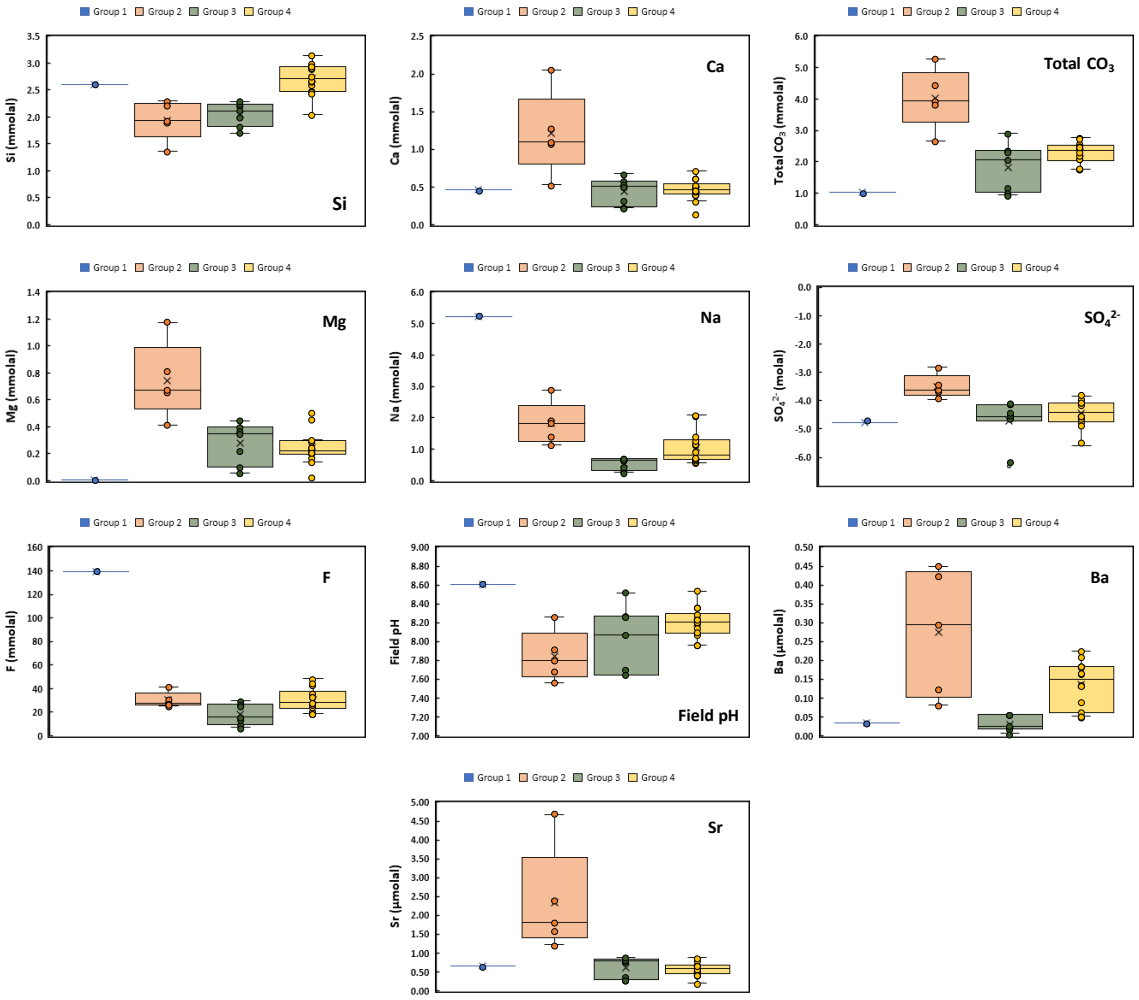

Figure 5. Box-and-whisker plot of groundwater chemistry in samples from Groups 1, 2, 3, and 4. Individual samples are represented by circles; boxes represent second quartile of each Group data with the median plotted as the horizontal line within each box; whiskers above and below each box represent 1st and 3rd quartiles of each Group data.

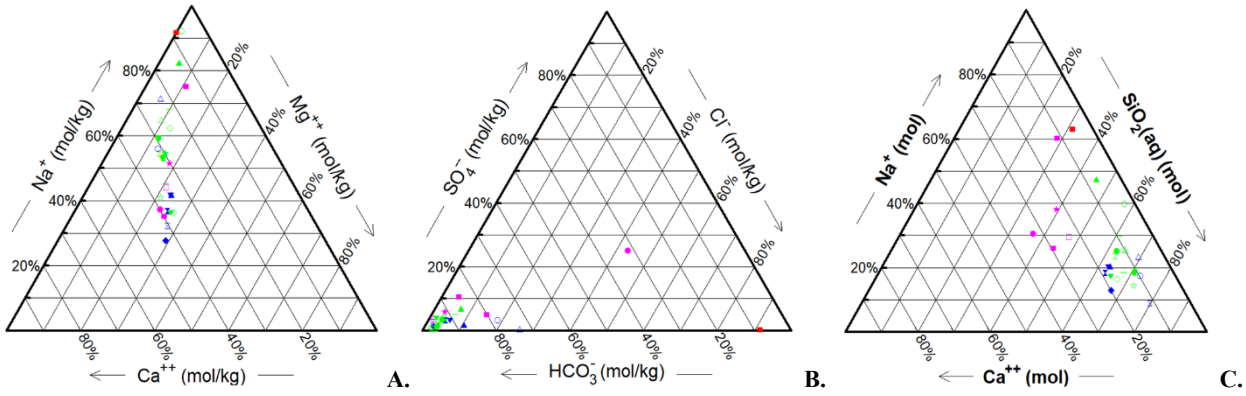

Figure 6. Ternary diagram of water composition (in molal): A. Na-Mg-Ca, B. SO_4-Cl-HCO_3 C. Na-SiO_2-Ca. Colors refer to sample Group number (red = Group 1, pink = Group 2, blue = Group 3, green = Group 4).

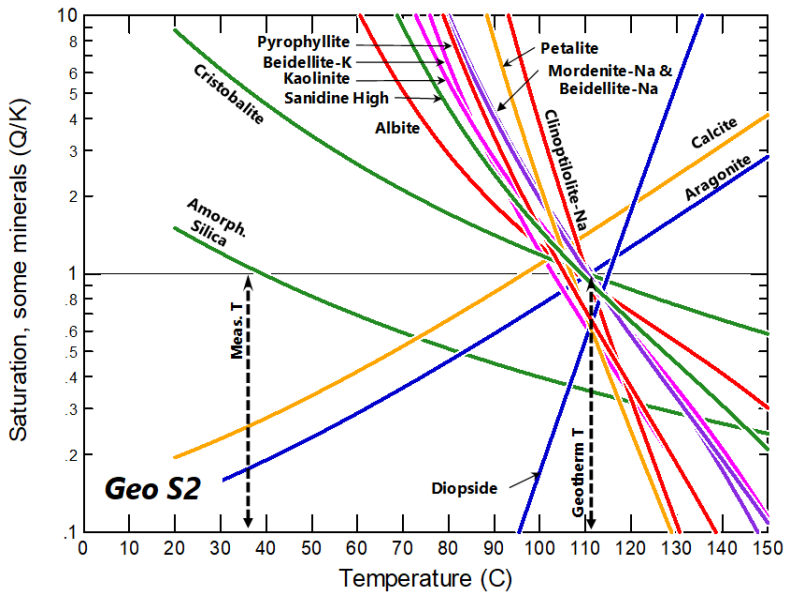

Figure 7. Saturation indexes versus temperature for Bingham Springs. Optimized for temperature and log(f[CO2]). Fe(III) calculated from amorphous $Fe(OH)_3$ equilibrium. Geothermometric temperature estimated to be 111.4 ±0.2° C.

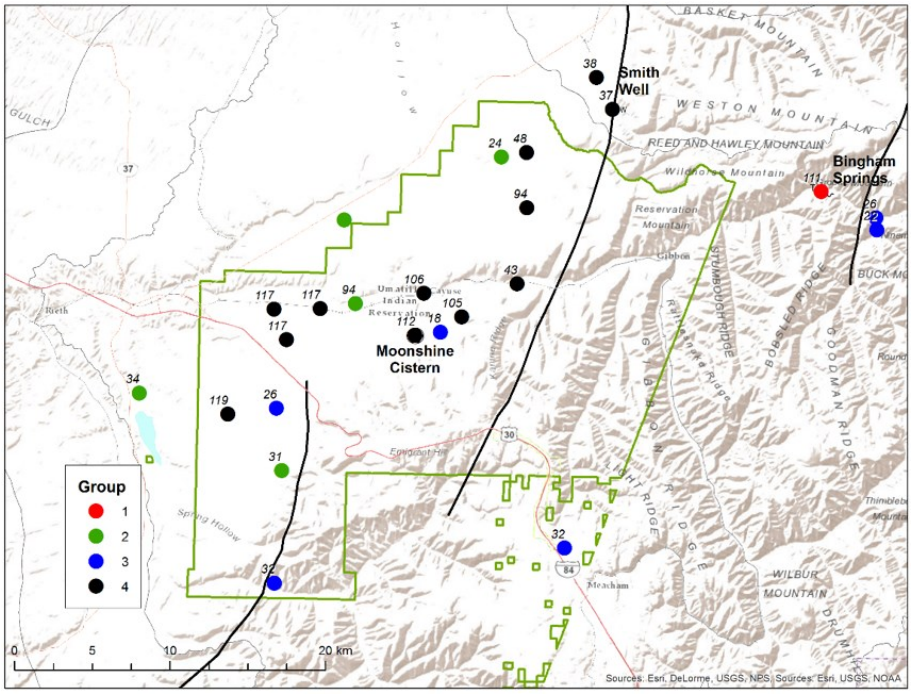

Figure 8. Locations of samples collected for analyses of aquatic chemistry and geothermometry. Group numbers were identified in the Cluster Analysis. Geothermometry temperatures are shown next to each sample in °C. The green polygons define the borders of the UIR.

Given the estimated thickness of 274 m for the two basalt flows of the undifferentiated Grande Ronde in the Birch Creek drainage, and assuming constant thickness of these flows between the two sites, we estimate that MW-6 would need to be about 234 m deeper, or a total depth of about 610 m, to reach below the CRBG into the underlying formations. Since the well head elevation of MW-6 is about 480 m, the elevation of the CRBG base would be about 130 m BMSL. As noted above, the elevation of the CRBG base at Birch Creek is 864 m, implying a vertical offset of over 970 m across the structure (fault or fold) responsible for uplifting

the Blue Mountains and which lies between these two sites. The Birch Creek site is 3 km southeast of the Hawtmi Fault (in the upthrown block), and MW-6 is 2.5 km west of the Hawtmi Fault (in the down dropped block).

4. GEOTHERMAL RESOURCE POTENTIAL MODEL

Geothermal resource potential was assessed using the methodology of the Washington State Play Fairway Analysis (PFA) developed by the Washington Geological Survey (Norman et al, 2015; Forson et al., 2017). All the data was loaded into an ArcGIS mapping platform to determine the relative position of geothermal resource indicators on and near the UIR, normalized from 0-1 based on geothermal favorability criteria specific for each data type, and interpolated to create continuous rasters for the various datasets. The rasters were then clipped to the PFA model area around the CTUIR, which is the same extent of the MT survey. The rasters were grouped into three categories of geothermal resource indicators 1) heat, 2) permeability, and 3) fluids/cap, and were weighted and combined using consensus based, expert guided, fuzzy logic within each category and then for all three to create a final map of geothermal favorability. Various criteria/weighting for data uncertainty were used for certain datasets, but overall model uncertainty was assumed to be considered by the expert panel when they decided on the weighting for each data type.

4.1 Analytical Hierarchy Process

Geothermal favorability is represented in maps of the UIR rendered using ArcGIS. Geologic and geophysical data used to determine favorability are input to these maps as layers which have been normalized and weighted using the Analytical Hierarchy Process (AHP) (Saaty, 2008; Goepel, 2013). The AHP is a valuable tool for making complex decisions using a variety of different data types by quantitatively ranking those data groups in a series of pairwise comparisons. The AHP tests the internal consistency of each decision maker's evaluations, which reduces bias in the decision-making process. Here the AHP was used to compare and weight the value of the proxies for geothermal favorability to produce an integrated prediction of resource potential. Each of the experts involved in this project (e.g., USGS, ARE, and CTUIR) contributed to the AHP process to weight the parameters in order of importance to the favorability model. As the individual expert valuations are combined to generate the overall weights for each of the parameters, the process generates alerts if the opinions are consistent with each other or if team members strongly disagree. In such cases, the AHP process was reiterated in round table discussions among team members to reweight input parameters until there is sufficient agreement.

4.2 Heat

Heat potential was assessed using three datasets: 1) surface spring temperature compiled from the Geothermal Information Layer for Oregon (GTILO) and the Washington Geologic Information Portal (WGIP) 2) heat flow measurements compiled by the Southern Methodist University (SMU) Geothermal Laboratory, and 3) the results of the geothermometry analysis (Figure 8). Quaternary volcanic vents and intrusive rocks are also considered indicators of geothermal favorability but since none exist in the area these layers were left out. Table 1 has the criteria for converting the heat data to favorability and Table 2 has additional weighting criteria for heat flow measurements as a measure of uncertainty. Because of the topography across the UIR, it is important to give greater weight to heat flow measurements that are below the mean surface elevation of 711 m AMSL because they are more representative of background heat flow for the area. The calculated geothermometers (Figure 8), measured heat flows, and spring temperatures were interpolated across the region using Inverse Distance Weighting.

Table 1. Weighting for heat favorability

Data Layer	Criteria	Weight
heat flow	<50 mW/m^2	0
	>100 mW/m^2	1
thermal springs	<10° C	0
	>75° C	1
geothermometry	<20° C	0
	>120° C	1

Table 2. Weighting for heat flow measurements.

Depth below surface (m)	Weight
<0	0.25
0-100	0.5
100-250	0.75

4.3 Permeability

Permeability favorability was based on layers of fault density and slip/dilation tendency which depends on fault orientation and stress. Fault density implies that faults and fractures act as permeable conduits for geothermal fluid circulation, and that closely spaced faults and fault intersections cause more intense fracturing that is highly permeable. Slip tendency (T_s), which is the shear stress (τ) to normal stress (σ_n) ratio on a fault surface calculated from the remote stress describes the likelihood that a fault is experiencing continuous slip that maintains fault permeability, or if older structures have the potential to be re-activated in the current stress field and become permeable conduits:

$$T_s = \tau / \sigma_n \qquad \text{eq. 2}$$

Dilation tendency (T_d) is the ratio of the difference between the maximum principal compression (σ_1) and the normal stress, and the difference between σ_1 and the minimum principal compression (σ_3). It can be used to assess the potential for a structure to dilate and therefore carry higher volumetric flowrates due to significant increases in fault transmissivity from opening:

$$T_d = (\sigma_1 - \sigma_n)/(\sigma_1 - \sigma_3) \qquad \text{eq. 3}$$

Fault density was interpolated by Kernel density with a search radius of 1,500 m. Five fault datasets were used to create raster layers that were weighted by the AHP;

1. Faults from the UIR geologic map (Ely and Mehta, 2013) contain faults compiled from the Oregon Department of Geology and Mineral Industries (DOGAMI), and have certainty criteria based on workers assessment or fault quality (i.e. certain, approximate, approximate and queried, concealed, and inferred);
2. Faults from the USGS QFFDB were used with certainty criteria based on fault recency, or age, with more recent faulting weighted higher;
3. Fault lineations were interpreted from alignments of maxima in maximum horizonal gradients of gravity anomalies. These maxima approximately overlie near-vertical contacts between rocks of contrasting density (Blakely and Simpson, 1986). Alignments were assigned certainty based on the magnitude of the horizontal gradient.
4. Faults from aeromagnetic data had certainty weighting based on lineations that are known to be faults, and other contacts of possible structural significance ("structure") which are weaker lineations that could potentially be faults.
5. Dikes are distinguished from faults in aeromagnetic data by closely spaced intense magnetic highs that strike in the same direction as known regional dike swarms that fed the CRBG.

4.4 Magnetotellurics

MT conductivity can vary as a function of hydrothermal clay alteration and brine salinity and fluid temperature (Peacock et al. 2018). MT resistivity values ranging from less than 10 ohm-meters were assigned a geothermal favorability of one, and those greater than 200 ohm-meters were assigned a favorability of zero based on comparison with geothermal project data collected form the Darajet, Kakkonda, Wairakei, Ciero Prieto, and the Salton Sea. The maps of normalized MT data used for each layer can be found in Peacock et al., 2018.

4.5 Analytical Hierarchy Process Results

After data was normalized using favorability and certainty criteria, they were multiplied by their AHP weights and summed within the three categories. Results for all three categories were then combined using AHP weights that compare the three categories. The final map produced (Figure 12) shows overall geothermal favorability across the UIR.

4.5.1 Heat

Table 3 summarizes the AHP results for the heat layers, and Figure 9 is a map of geothermal favorability based on heat data. The geothermometry was weighted the highest because the sampling and analysis was specifically done for the UIR. It also has the highest density of data points within the UIR. The heat flow layer was weighted the lowest because there are only two data points within the model area, and the one to the east is drilled at higher elevation where downflow may have swept heat away so the site may not be representative of background heat flows. The spring temperatures scored far lower than the geothermometry because the data is also sparse, but twice as high as the heat flows because they are measured at known thermal springs such as the Bingham Springs nearby to the east, and the Hot Lake Springs further to the southeast. The most favorable areas in the heat data are in the western part of the UIR, because this is where the highest temperature geothermometry is located.

Table 3. AHP weighting of heat layers

Input data layer	Brief description	Weight
heat flow measurements	From SMU database, two measurements on UIR, three more nearby. Total of 50 measurements interpolated over ~20,000 km^2.	0.123
spring temperature	From GTILO and WGIP. Closest measurement from Bingham Springs to the east of UIR, with two more nearby to the south. Total of 43 measurements interpolated over ~60,000 km^2.	0.255
geothermometry	Sampled/analyzed 2017. 16 measurements on UIR and 7 measurements ~5-10 km from UIR. Total of 24 measurements interpolated over 1,600 km^2.	0.622

4.5.2 Permeability

The top five rows in Table 4 are the five fault types interpolated using kernel density. After these layers were weighted against slip and dilation tendencies, their weights were normalized for weighting within the slip and tendency layers, which was done for all the faults. The layer with faults drawn from the high resolution aeromagnetic survey had the highest AHP weight because these data: 1) represent deep geophysical signals on known quaternary faults (weighted second highest), and 2) reveal both buried faults and mapped older faults (weighted third highest) such as the buried northern continuation of the Hawtmi fault zone, and the Wilahatya fault zone (Figure 10). Slip and dilation tendency data were weighted lowest due to relatively quiescent tectonics of the area.

Table 4. AHP weighting of permeability layers

Input data layer	Brief description	Weight	Normalized weight for slip/dilation tendency
aeromag faults/structure	magnetic lineations that have orientations, amplitude, and shape similar to known fault systems in the area.	0.287	0.326
aeromag dikes	numerous closely spaced parallel magnetic lineations trending north-northwest.	0.124	0.141
gravity faults	lineations defined by the alignment of horizontal gravity gradient map spots.	0.106	0.120
USGS faults	faults from the QFFD with attributes of fault age and slip sense.	0.197	0.224
geologic faults	faults in UIR geologic map created in 2013 sourced from DOGGR	0.167	0.190
slip tendency	fault segments likely to slip under current stress conditions	0.059	
dilation tendency	fault segments likely to dilate under current stress conditions	0.060	

4.5.3 Magnetotellurics

The MT layer with the highest weight is 2,032 m BMSL (ca 2.5 km below Moonshine Cistern) which is inferred to represent hydrothermal brine or hydrothermally altered clays which are drilling-accessible (Table 5). The 2nd highest weighted layer is 1,092 m BMSL, which looks like a clay cap bottom and contains the most conductive anomaly (0.5 ohm-meters) under the intersection of the Wilahatya fault zone and the Thorn Hollow Fault zone (Figure 11). It is practical that these two layers were weighted highest because their interface would be the most logical target for geothermal wells, though the exact horizon is not well defined by this study.

Table 5. AHP weighting of cap and fluids layers

Input data layer	Brief description	Weight
392 mbsl (~1 km deep)	shallow hydrothermal clay alteration	0.073
1,092 mbsl (~1.5 km deep)	deep hydrothermal clay alteration	0.290
2,032 mbsl (~2.5 km deep)	shallow conductive hydrothermal brine	0.352
3,582 mbsl (~4 km deep)	deep conductive hydrothermal brine	0.286

4.6 Overall Geothermal Favorability

The main input layers were weighted fairly equally; the cap and fluids and heat layers were weighted higher than the permeability layers (Table 6) because the area is tectonically quiescent. Overall geothermal favorability was mapped across the UIR (Figure 12) based on combined AHP weighted data. The eight most favorable locations for thermal gradient boreholes (TGHs), ranked from 1 to 8 in the PFA model, are also identified on Figure 12. These results present multiple testable hypotheses for the nature of the geothermal reservoir and should help guide a strategy for exploratory drilling. Drilling TGHs are considered one of the key next steps in confirming the magnitude and extent of a geothermal resource below the UIR.

Table 6. AHP weighting for combined favorability

Input data layer	Weight
heat	0.371
permeability	0.23
cap and fluids	0.399

***Primary* Favorability Sites for UIR**

1) Near the intersection between the Wilahatya fault zone and the Thorn Hollow fault zone;
2) The area near the Moonshine Cistern, with smaller shoulder peaks; and
3) 3 km west-southwest of Moonshine Cistern along the Wilahatya fault zone.

***Secondary* Favorability Sites for UIR**

4) 6 km east-northeast of Moonshine Cistern along the Wilahatya fault zone.
5) near the northern tip of the Hawtmi fault zone;
6) (and 7) 5-6 km north of the Moonshine Cistern near the southern tip of the dike swarm; and
8) 11.5 km due west from the Moonshine Cistern near a cluster of high geothermometers and the deepest MT anomaly.

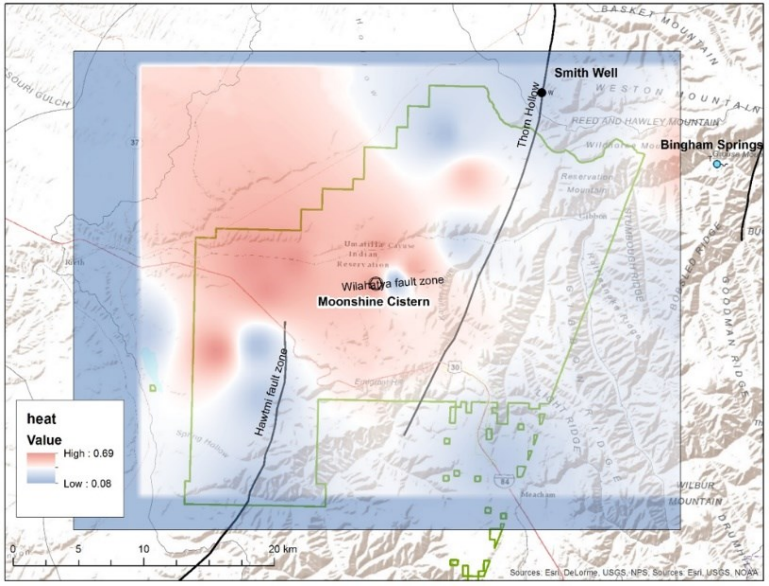

Figure 9. Geothermal favorability based on AHP weighted heat data.

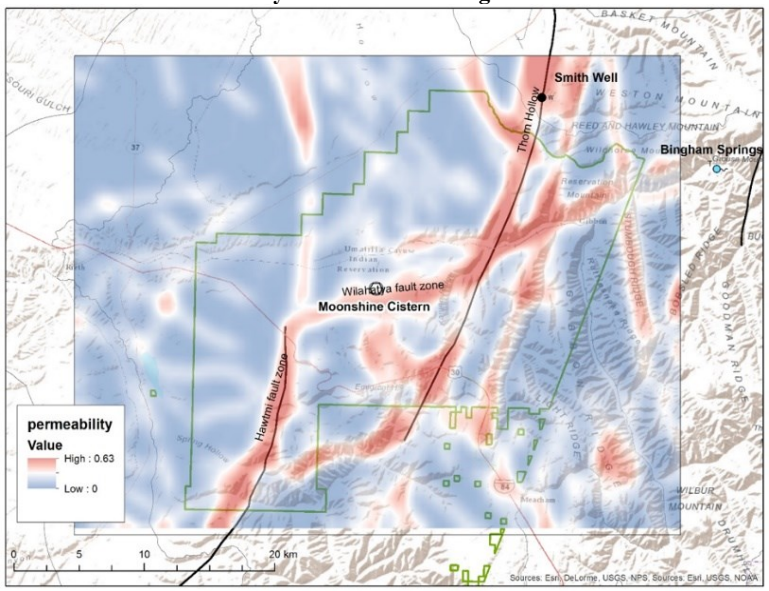

Figure 10. Geothermal favorability based on AHP weighted permeability data.

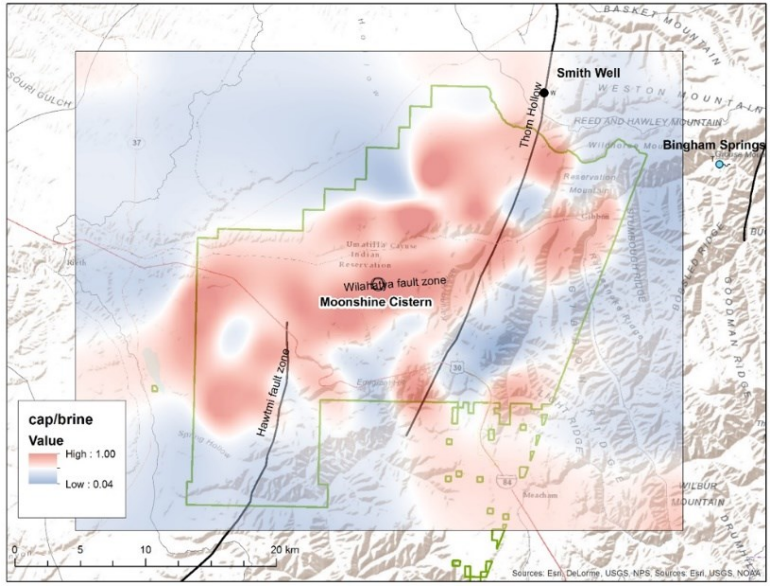

Figure 11. Geothermal favorability based on AHP weighted magnetotelluric data.

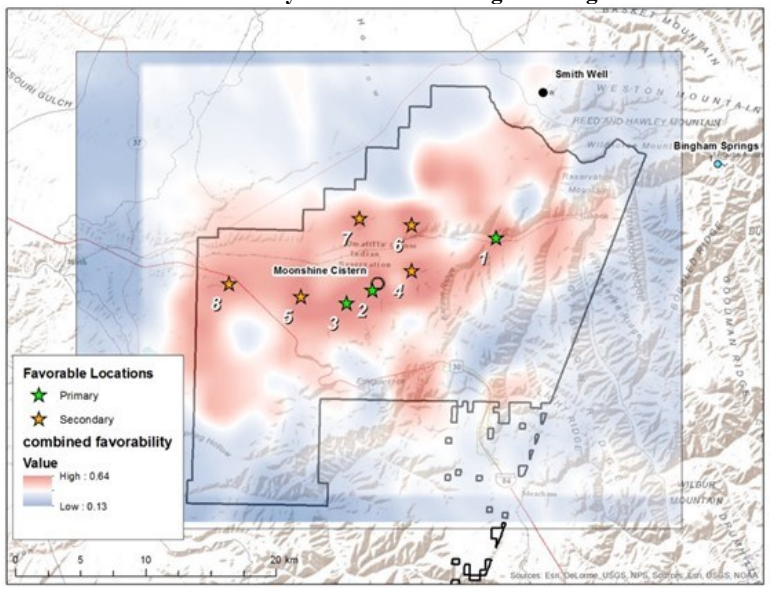

Figure 12. Overall geothermal favorability and eight best TGH location candidates.

5. DISCUSSION

The previous sections described the synthesis of new and existing geophysical and geological data using the methods of Analytical Hierarchy Process (AHP) and expert opinions. The result is the combined geothermal favorability map (Figure 12), and most favorable locations for drilling TGHs to confirm the magnitude and extent of a heat resource. This section presents the implications and a potential explanation for the favorability results, the remaining unknowns, and how to test the hypotheses implied by the favorability map in subsequent exploration.

5.1 Current Conceptual Model of Potential Geothermal Resource

The source of geothermal heat beneath the UIR is assumed to be non-magmatic and probably derived from radiogenic heat production in basement rocks below the CRBG. These assumptions arise from the geologic age and tectonics of the region, low estimated heat flow, and lack of recent volcanism in the area. Geothermometry analysis found evidence of geothermal impact in shallow groundwater at temperatures that could be utilized as a direct-use heating resource. Hotter, more valuable, and potentially power producing resources should exist below these warm resources. Whether these hotter deeper resources are accessible is controlled by the geothermal gradient, i.e., temperature change with depth. Measuring the geothermal gradient beneath the UIR would be a top priority of the next phase of geothermal resource assessment.

A potential but speculative model of the hydrothermal system below the UIR is illustrated in Figure 13, as presented in Ritzinger et al., 2018. This model is consistent with the data and analysis presented in this report, and it can serve as a hypothesis to evaluate new field data collected during further geothermal resource assessments (e.g., thermal gradient boreholes, referred to as temperature gradient holes later in this report).

It begins with meteoric water infiltration in the highlands of the Blue Mountains. Water gains heat and buoyancy as it descends through deep-seated crustal faults and major fault intersections. With added buoyancy, the water migrates north and west away from the Blue Mountains into the central area of the UIR – the region of higher geothermal favorability shown. Faults along the Wilahatya fault system may tap deep thermal reservoir fluids at fault intersections and provide potential access to those fluids at relatively shallow depths. It is those zones that have been identified as the most favorable locations.

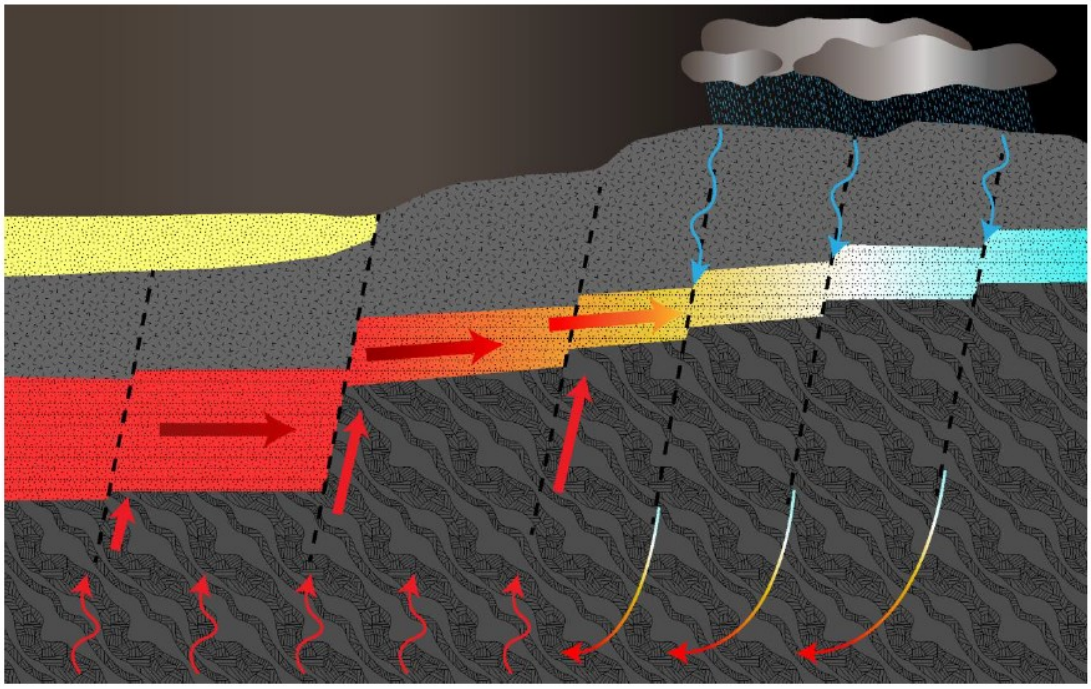

Figure 13. Cartoon illustration of conceptual model for UIR (Ritzinger et al., 2018). Cross Section view along an NW-SE profile obliquely crossing the Wilahatya fault zone. Infiltrating meteoric fluids recharge the reservoir along structures in the highlands of the Blue Mountains that penetrate overburden, the CRBG, and underlying basement. Discrete structural intersections that enhance porosity along the Wilahatya and Hawtmi fault systems provide conduits for fluids to migrate vertically from the reservoir to shallow depths, while permeable layers within the basement and sediment packages accommodate lateral flow from northwest to southeast.

5.2 Unknowns / Risks

The geothermal favorability map is a synthesis of available data. Although not unique or well-tested, the conceptual model above is consistent with the data sets collected. Some of the important data gaps remaining include:

1. **Stress regime.** The principle stress magnitudes and directions used (Section 3) are not locally constrained or measured but are derived from regional models. Local measurements are needed to better understand the stress resolved onto faults and fractures and thus fracture permeability. The best stress measurements are taken from boreholes.
2. **Neotectonics.** The current stress regime can also be partially derived from characterization of active faulting. No active faults have been identified in the immediate area of the UIR, but this may be due to lack of good data.
3. **Heat flow.** Only two heat flow measurements taken at the margins of the area of interest were used in the heat model and are of unknown quality. Heat flow can be determined from a temperature gradient hole (TGH) that reaches depths below flowing aquifers where heat flow is conductive.
4. **Columbia River Basalt Group thickness.** The CRBG is over 3,000 m thick where it filled a Miocene basin near Yakima, WA, 110 miles northwest of the UIR (Reidel et al., 2013). The CRBG under the UIR is believed to be much thinner (ca 600 – 1,000 m), but no borehole has yet penetrated the full thickness of these basalts within the UIR.
5. **What's below the CRBG?** In the Birch Creek drainage there is a small window into the rocks and structures below the CRBG. Further information about the extent and in situ characteristics (permeability, porosity, fluids) of pre-CRBG units is needed because they are the likely geothermal reservoir rocks.

7. REFERENCES

Barry et al. 2013. Eruption Chronology of the Columbia River Basalt Group; GSA Special Paper 497, 45-66.

Blakely, R. J. and R. W. Simpson, 1986. Approximating edges of source bodies from magnetic or gravity anomalies. Geophysics, vol. 51, p. 1494-1498.

CTUIR, 2017. Sampling and Analysis Plan for Geothermal Indicators in Water. Confederated Tribes of the Umatilla Indian Reservation (CTUIR), Department of Natural Resources Energy & Environmental Sciences Program, 22pp.

Ely, K., and S. Mehta, 2013. Geologic Framework of the Upper Umatilla River Basin and Extended Area. Confederated Tribes of the Umatilla Indian Reservation, Unpublished manuscript, 53 p.

Ferns, M.L., V.S. McConnell., and I.P. Madin, 2006. Geology of the upper Grande Ronde River basin, Union County, Oregon by Mark L. Ferns, Vicki S. McConnell, and Ian P. Madin, 2006, 85 p., Plate 1, 1:125,000; Plate 2, 1:100,000. Open File Report 2006-19.

Forson, C., A. Steely, T. Cladouhos, M. Swyer, N. Davatzes, M. Anderson, B. Ritzinger, J. Glen, J. Peacock, W. Schermerhorn, E. Burns, and P. Stelling. 2017. Geothermal play-fairway analysis of Washington State prospects: Phase 2 technical report. U.S. Department of Energy Geothermal Technologies Program, Award no. DE-EE0006728.

Goepel, K.D., 2013. "Implementing the Analytic Hierarchy Process as a standard method for multi-criteria decision making in corporate enterprises—A New AHP Excel Template with Multiple Inputs" Proceedings of the International Symposium on the Analytic Hierarchy Process 2013.

Heidbach, O., M. Rajabi, K. Reiter, M. Ziegler, WSM Team, 2016. World Stress Map Database Release 2016. GFZ Data Services, doi:10.5880/WSM.2016.001.

Jenks, M.D., P.E. Staub, M.L. Ferns, I.P. Madin, L. Ma. R.P. Geitgey, 2005. Oregon geologic data compilation [OGDC], release 1 (northeast Oregon). Superseded by OGDC-6, Oregon Geologic Data Compilation, release 6, compiled by Rachel L. Smith and Warren P. Roe.

Kuehn, S.C., 1995. The Olympic-Wallowa Lineament, Hite Fault System, and Columbia River Basalt Group Stratigraphy in Northeast Umatilla County, Oregon. Master's Thesis Washington State University.

Madin, I.P., and R.P. Geitgey, 2007. Preliminary geologic map of the Umatilla Basin, Morrow and Umatilla Counties, Oregon. Open File Report 2007-15.

McCaffrey, R., A.I. Qamar, R.W. King, R. Wells, G. Khazaradze, C.A. Williams, C.W. Stevens, J.J. Vollick, and P.C. Zwick. 2007. Fault locking, block rotation and crustal deformation in the Pacific Northwest. Geophysical Journal International, v. 169, no. 3, p. 1315-1340.

Norman, D.K., C. Forson, J.L. Czajkowski, M.W. Swyer, T.T. Cladouhos, G.M. Schmalzle, and N.C., Davatzes. 2015. Geothermal play-fairway analysis of Washington State prospects: Phase 1 technical report. U.S. Department of Energy Geothermal Technologies Program, Award no. DE-EE0006728.

Palmer, C., 2018. Umatilla Indian Reservation Geothermometry. Unpublished report, 40pp., April.

Peacock, J. R., Glen, J., Ritzinger, B., Earney, T., Schermerhorn, W., Siler, D., Anderson, M., 2018, Geophysical Imaging Geothermal Systems Spanning Various Geologic Settings, Geothermal Resource Council Transactions, 42, 1369-1382.

Reidel, S. P., V.E. Camp, T.L. Tolan, and B.S. Martin, 2013. The Columbia River flood basalt province: Stratigraphy, areal extent, volume, and physical volcanology. GSA Special Paper 497, 45-66.Saaty, T.L., 2008. “Decision making with the analytical hierarchy process” International Journal of Service Sciences, v. 1, no. 1, p. 83-98.

Ritzinger, B., J. Glen, J. Peacock, R. Blakely, P. Mills, L. Staisch, S. Bennett, and B. Sherrod, 2018. Geothermal Potential of the Umatilla Indian Reservation, Oregon: Evidence from Detailed Geophysical Investigations. Geothermal Resource Council Transactions, 42, 925-942.

Schwartz, J. et al., 2009. Analysis of the Wallowa-Baker terrane boundary: Implications for tectonic accretion in the Blue Mountains province, northeastern Oregon. GSA Bulletin, 122(3/4), 517–536.

Ussher, G., C. Harvey, R. Johnstone, E. Anderson, 2000. Understanding the Resistivities Observed in Geothermal Systems. Proceedings World Geothermal Congress, Kyushu – Tohoku, Japan, May 28 – June 10, 2000.

Wong, I., and J. Bott, 1995. A look back at Oregon's earthquake history, 1841–1994: Oregon Geology, v. 57, no. 6, p. 125–139.

Zhu, T. Y., 2012. Some useful numbers on the engineering properties of materials (geologic and otherwise). GEOL 615 Course Materials, Department of Geophysics, Stanford University.